

Encapsulated Silicon Nitride Nanobeam Cavity for Hybrid Nanophotonics

Taylor K. Fryett,[†] Yueyang Chen,[†] James Whitehead,[†] Zane Matthew Peycke,[‡] Xiaodong Xu,^{‡,§} and Arka Majumdar^{*,†,‡}

[†]Electrical Engineering, University of Washington, Seattle, Washington 98189, United States

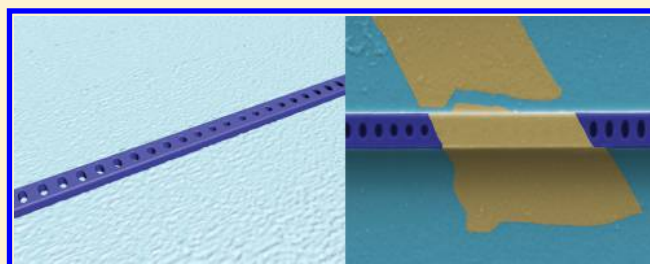
[‡]Department of Physics, University of Washington, Seattle, Washington 98189, United States

[§]Materials Science and Engineering, University of Washington, Seattle, Washington 98189, United States

Supporting Information

ABSTRACT: Most existing implementations of silicon nitride photonic crystal cavities rely on suspended membranes due to their low refractive index. Such floating membranes are not mechanically robust, making them suboptimal for developing a hybrid optoelectronic platform where new materials, such as layered 2D materials, are transferred onto prefabricated optical cavities. To address this issue, we design and fabricate a silicon nitride nanobeam resonator where the silicon nitride membrane is encapsulated by material with a refractive index of ~ 1.5 , such as silicon dioxide or PMMA. The theoretically calculated quality factor of the cavities can be as large as 10^5 , with a mode-volume of $\sim 2.5(\lambda/n)^3$. We fabricated the cavity and measured the transmission spectrum with the highest quality factor reaching 7000. We also successfully transferred monolayer tungsten diselenide on the encapsulated silicon nitride nanobeam and demonstrated coupling of the cavity with both the monolayer exciton and the defect emissions.

KEYWORDS: Photonic crystal cavity, layered materials, hybrid nanophotonics



Silicon nitride (SiN) offers several advantages over silicon for building photonic integrated circuits due to its large band gap. For instance, two-photon absorption in SiN is negligible at the telecommunication wavelengths. This allows operation at much higher optical power and with significantly lower loss compared to similar silicon devices. The thermo-optic effect in SiN is also an order of magnitude smaller compared to silicon and could potentially provide a scalable integrated photonic platform that is far less susceptible to thermal fluctuations. However, a major problem with SiN is that its carrier densities cannot be modulated easily due to its large bandgap, resulting in a lack of active devices. This problem is worsened by the amorphous nature of SiN grown via plasma enhanced and low pressure chemical vapor deposition (PECVD and LPCVD), which makes integration of other active materials by epitaxial growth more difficult. For example, complex electro-optic oxides¹ or quantum confined structures,² which can be grown or wafer-bonded on silicon, cannot be integrated on SiN without compromising the material performance. In contrast, layered 2D materials including graphene and transition metal dichalcogenides (TMDCs) can adhere to any substrate via van der Waals forces. This removes the explicit lattice matching requirement of epitaxial growth, making this class of materials promising for developing hybrid integrated SiN platform.^{3,4}

Recently demonstrated graphene integrated SiN micro-ring electro-optic modulators attest to the potential of a hybrid integrated platform.⁵ Transition metal dichalcogenides have also been integrated on SiN micro-ring and disk resonators to explore the Purcell effect.^{6–8} However, all previous work on 2D material clad SiN resonators focused on whispering gallery mode resonators. Photonic crystal (PhC) resonators are often preferred due to their small mode-volumes (V_m). Cavity enhanced photoluminescence (PL),^{9–11} electroluminescence,¹² and second harmonic generation^{13,14} in layered materials have already been demonstrated using silicon and gallium phosphide PhC resonators. Unfortunately, the small refractive index of SiN ($n \approx 2$) inhibits the opening of a complete band gap in two-dimensional photonic crystals for common 2D lattice geometries such as hexagonal and square lattices. This difficulty is the primary reason why many in the community use 1D photonic crystal nanobeam structures where bandgaps are more readily opened.¹⁵ The low refractive index of SiN also makes the design of SiN PhCs more difficult than the design of PhCs in materials with higher refractive index such as silicon. This is why all previously reported SiN PhCs are suspended, as air provides a greater index contrast than other common dielectrics such as SiO₂. The low index of SiN also exaggerates the

Received: January 8, 2018

Published: April 18, 2018

detrimental effects of asymmetries in the refractive index profile. For example, our numerical simulations suggest that a traditionally designed suspended SiN nanobeam¹⁶ with a quality factor of $\sim 3 \times 10^5$ completely loses its resonance when placed on an oxide substrate. The cavity mode can be recovered, albeit with significantly reduced quality factor (~ 1000), when the SiN nanobeam is embedded in a material with refractive index of ~ 1.5 . However, an outstanding challenge presented by floating membranes is its propensity to be damaged by common microfabrication techniques such as resist spinning for lithographic overlay. The popular dry transfer techniques for building van der Waals heterostructures^{16,17} can also easily destroy floating membranes (see Supporting Information). While one can realize hybrid devices without transferring the layered materials, as recently reported,¹⁷ it is difficult to integrate different 2D materials on the same photonic chip, and the resulting floating membranes still remain susceptible to damage from further fabrication steps. Finally, for rapid prototyping and initial characterization of the layered material clad cavities, the 2D materials must be removed using the same dry transfer methods used to initially deposit the material followed by vigorous sonication. Therefore, the mechanical stability of an encapsulated nanobeam is particularly attractive for a hybrid photonic platform.

In this article, we design and fabricate a SiN nanobeam cavity encapsulated inside a medium of refractive index ~ 1.5 (Figure 1) to address the need for mechanical stability in a hybrid

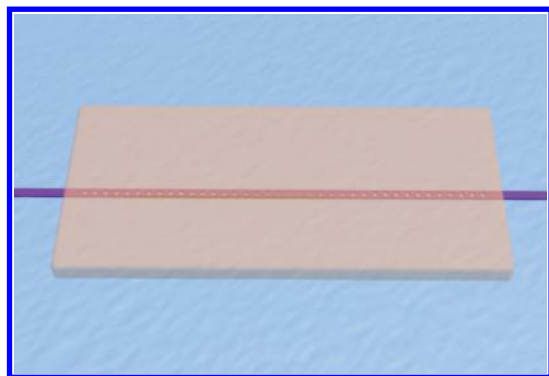


Figure 1. Schematic of the encapsulated SiN nanobeam resonator: The SiN nanobeam resonator sits on an oxide substrate to provide the mechanical stability. The nanobeam is also covered with PMMA to provide the z -symmetry often necessary to support a high quality factor TE mode.

photonic platform. The encapsulation provides the additional benefit of material passivation for long-term stability of less stable layered materials such as black phosphorus,¹⁸ and MoTe₂.¹⁹ Via numerical simulations, we found that our designed cavity can reach a quality (Q) factor of $\sim 10^5$ and a mode volume of $\sim 2.5(\lambda/n)^3$. Experimentally, we measured a Q -factor of up to ~ 7000 in transmission (see Supporting Information). We also demonstrated integration of monolayer tungsten diselenide (WSe₂) with the nanobeam cavity and observed the cavity coupled PL. Our work presents a new way to build hybrid 2D material–cavity photonic circuits using low-mode-volume SiN resonators.

DESIGN OF THE RESONATOR

To design the nanobeam optical resonators, we first simulated the band structure of a SiN ($n \approx 2$) 1D photonic crystal with

surrounding medium of $n \approx 1.47$ using the MIT photonic bands (MPB) software package.²⁰ We utilized elliptical holes, following the example of a previously reported design.²¹ Figure 2a shows the resulting band diagram, which includes the

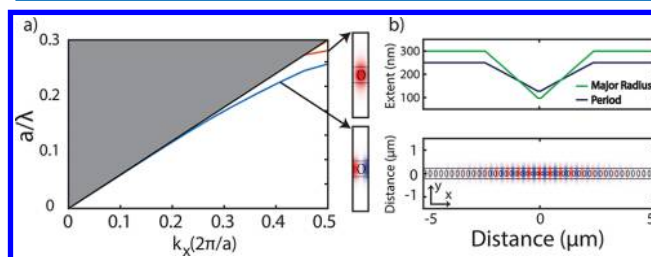


Figure 2. Design of the encapsulated SiN nanobeam cavity: (a) band diagram of the 1D photonic crystal, where the SiN has a refractive index of 2, and the surrounding medium has a refractive index of 1.47. We denote a to be the periodicity of the photonic crystal and λ as the wavelength. The profiles of E -field along y -direction for each band are also shown. (b) Cavity is realized by linearly decreasing the hole's major radius as well as the hole spacing. An image of the resulting localized field (E_y) is overlaid with the nanobeam edges for clarity.

air band, the dielectric band, and the field distributions at the band-edges. Once a suitable band structure was found we moved to tuning a lattice defect to create a resonator using the finite-difference time-domain (FDTD) solver from Lumerical, Inc. Specifically, we created the cavity by linearly tapering the major axis diameter of the holes and the period (Figure 2b) about the cavity center. We optimized our design parameters until we found a suitably high quality factor ($Q \approx 10^5$) resonance centered at 740 nm. In our design, the nanobeam had a thickness $t = 330$ nm and a width of $w = 450$ nm. The Bragg region consisted of 40 elliptical holes placed at a period $a = 233$ nm. These elliptical holes have a major and minor diameter of 300 and 100 nm, respectively. The innermost elliptical holes have a major diameter of 100 nm and were separated by 140 nm. The resulting electromagnetic mode has a mode volume of $\sim 2.5(\lambda/n)^3$, a factor of five larger than previously reported floating SiN nanobeam resonators.^{16,22} However, to accommodate two grating couplers and their associated tapers within the field of view within our confocal microscope, the overall resonator size has to be reduced. To accomplish this, we reduced the number of Bragg periods to 20, resulting in a reduced quality factor of $\sim 15,000$.

NANOBEAM FABRICATION

We fabricated the nanobeam cavity using 330 nm thick SiN membrane grown via LPCVD on 4 μm of thermal oxide on silicon. The wafers are obtained from the commercial vendor Rogue Valley Microdevices. The refractive index of SiN is measured to be $n \approx 2$ using ellipsometry. We spun roughly 400 nm of Zeon ZEP520A, which was coated with a thin layer of Pt/Au that served as a charge dissipation layer. The resist was then patterned using a JEOL JBX6300FX with an accelerating voltage of 100 kV. The pattern was transferred to the SiN using a RIE etch in CHF₃/O₂ chemistry. Figure 3a shows the SEM of the fabricated SiN cavities on thermal oxide just after etching. To encapsulate the nanobeams, we spun poly(methyl methacrylate) (PMMA) at 2000 rpm, resulting in a coat approximately 1 μm thick. The chips were then baked at 180 °C to remove any remaining solvent. PMMA and PECVD silicon dioxide have similar refractive indexes,²³ however,

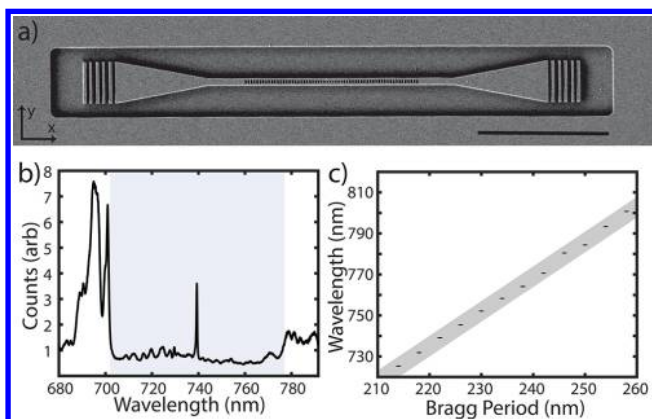


Figure 3. Bare cavity resonances: (a) SEM of a fabricated SiN nanobeam prior to encapsulation. The nanobeam resonators are probed via the two grating couplers on the ends of the nanobeams. The scale-bar is $10\ \mu\text{m}$. (b) Example cavity transmission spectrum as measured through the gratings. The shaded portion highlights the low transmission region from the Bragg reflectors, with the cavity peak at the center. (c) Observed cavity resonances scale linearly with the Bragg period, while holding the ratio between radii and periodicity constant.

PMMA is preferable for encapsulating the nanobeam in our experiments because it can be easily removed without any risk to the SiN nanobeams.

TRANSMISSION MEASUREMENTS

We then measured the transmission spectra of the optical resonators using a supercontinuum light-source (WhiteLase Micro from Fianium, Inc.). The supercontinuum light was

focused on one of the grating couplers, and the transmitted light was collected from the other grating and sent to a spectrometer (Princeton Instruments PIXIS CCD with an IsoPlane SCT-320 Imaging Spectrograph). The finest grating used in our experiment is $1200\ \text{mm}^{-1}$ blazed for $750\ \text{nm}$ with an estimated resolution of $\sim 0.06\ \text{nm}$. A cross-polarized setup is used to reduce the background, and we collect both TE and TM polarizations from the output grating. Figure 3b shows an example spectrum where the photonic bandgap and the cavity resonance ($Q \approx 2000$) are readily identified. Note that, as we did not have a tunable laser to measure the exact power transmission, we normalized the transmission using the transmission measured through a waveguide without any photonic crystal. To further confirm that the observed peak is indeed from a cavity, we measured several cavities with linearly scaled periods and major radii and observed the expected linear scaling of the cavity resonances (Figure 3c). The measured cavity Q factors fall within the 1500–7000 range. We attribute the one order of magnitude reduced quality factor in experiment compared to our simulations to fabrication imperfections, including nonuniformity of the hole sizes and side-wall roughness. We note that the cavities remain unaffected after removing, followed by respinning PMMA. We have tested the same chip through ten cycles of stripping and respinning of PMMA without observing any difference in the cavity spectra. We also extended our work to the telecommunication band, where we fabricated resonators with Q factors exceeding 10,000 (see Supporting Information).

INTEGRATION WITH LAYERED MATERIALS

After the initial characterization, we studied the layered material integration. Specifically, we chose to integrate monolayer WSe_2

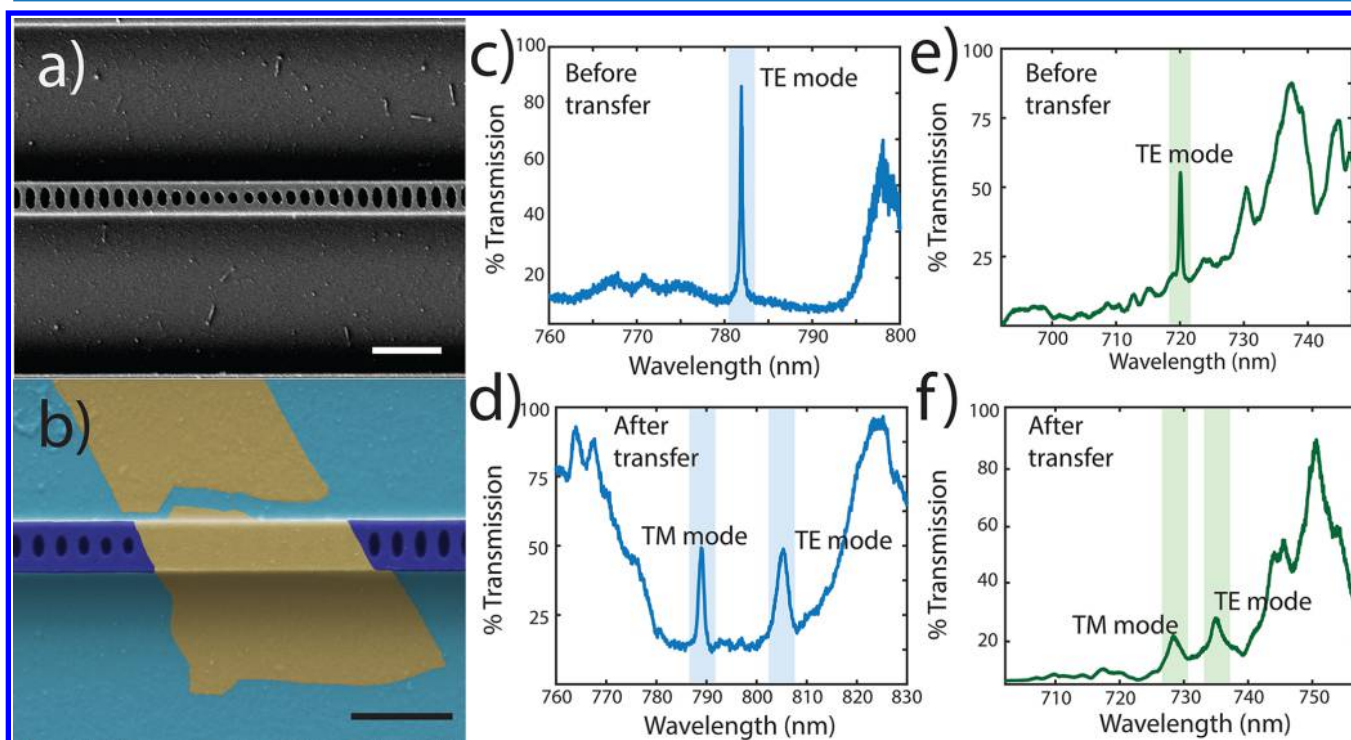


Figure 4. Transmission through SiN nanobeam before and after transfer of WSe_2 : (a) SEM of the defect region of the nanobeam. (b) False colored SEM of a nanobeam with monolayer WSe_2 . The SiN is shown in dark blue, the silicon oxide is shown in light blue, and the WSe_2 is shown in gold. The scale-bar in both figures corresponds to $1\ \mu\text{m}$. (c,e) Transmission spectrum before transferring WSe_2 for devices 1 and 2, respectively. (d,f) Transmission spectra after WSe_2 transfer for devices 1 and 2, respectively.

on a cavity with resonances within the exciton (device 1, shown in Figure 4c) and defect (device 2, shown in Figure 4e) spectral windows. The quality factors of these cavities without any integrated layered materials were 2,800 and 1,600, respectively. We note that, while several cavities with Q factor around ~ 7000 were measured (Supporting Information), they were not in the correct spectral window for integration with 2D materials or had low cavity transmission. The cavities were first stripped of the PMMA encapsulation and then flakes of monolayer WSe₂ were transferred on the SiN nanobeam cavities using the dry transfer method with a polycarbonate (PC) stamp.²⁴ We note that to completely remove the encapsulating PMMA, we perform vigorous sonication, which will destroy any suspended membranes. However, our cavities remain unaffected as they remain in contact with the substrate, attesting to their mechanical stability. Removal of the PC polymer, usually done with a solvent such as dichloromethane, carries an inherent risk of accidentally removing the transferred material. We avoided this risk by leaving the PC as transferred and adding a layer of PMMA to ensure proper encapsulation. Figure 4a shows the SEM of the cavity before WSe₂ transfer, and Figure 4b shows the SEM of the cavity with transferred 2D material. The SEM in Figure 4b is in false color to highlight the position of the WSe₂ monolayer.

As expected, the integration of 2D materials modifies the observed transmission spectrum. Figure 4d,f shows the transmission spectra of devices 1 and 2 with integrated 2D materials, respectively. The cavity modes are highlighted for clarity. The integration of 2D material red shifts the cavity resonances by ~ 25 and ~ 15 nm for devices 1 and 2, as well as reducing the Q factors to 800 and 400, respectively. The line width broadening after 2D material integration is expected due to the absorption from 2D materials.^{6,9,25} Additional broadening is also expected because the PC and WSe₂ prevent PMMA from filling some of the holes in the nanobeam near the cavity region. Our numerical simulations show that the Q factor of the cavity with several air-filled holes at the cavity region is expected to be ~ 2000 . The change in the refractive index profile will also affect the resonance wavelength of the nanobeam resonator. However, air-filled holes near the cavity center would cause a blue shift, rather than the observed red shift. We attribute this red-shift to the inclusion of PC, which has a slightly higher refractive index of ($n \approx 1.57$) than PMMA ($n \approx 1.47$). This was affirmed by additional FDTD simulations (see Supporting Information). We also found that this change caused a new cavity mode to appear at a slightly lower wavelength than that of the original mode. The appearance of the new mode is consistent with our experimental findings (Figures 4d,f). This additional mode is TM polarized (see the mode profiles in Supporting Information). We attribute the appearance of the TM mode to the slightly higher refractive index of PC breaking the z -symmetry. To further validate that this new mode appears due to the encapsulation with PC, we measured several nanobeams with PMMA. These same cavities were then stripped of PMMA, encapsulated with PC, and remeasured. We observed the appearance of the new mode and red shift of the cavity (see Supporting Information).

Measured PL from the devices confirmed cavity coupling with the monolayers. We measured the devices at 80 K and excited the monolayers from the top with a 532 nm CW laser diode with power of 40 μ W and beam spot with radius of 1 μ m. The resulting PL is collected from the grating couplers and sent to a spectrometer. We note that we performed PL experiments

on SiN devices with and without WSe₂ to confirm that the observed signal originates from WSe₂ and not the defect states in SiN.¹⁵ Figure 5a,b shows the resulting spectra for devices 1

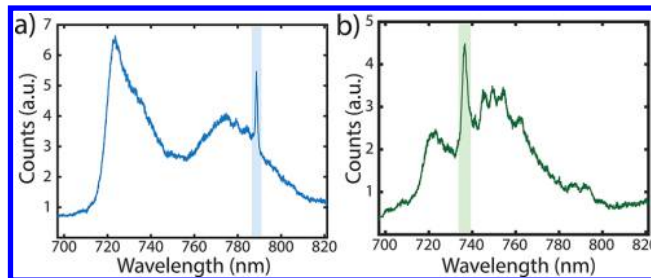


Figure 5. PL from the WSe₂ clad SiN nanobeam resonators: (a) PL from device 1 shows cavity coupled PL from the defects in WSe₂ monolayer and (b) PL from device 2 shows cavity coupled PL from the WSe₂ exciton.

and 2, respectively. The large background comes from the 2D material PL that leaks through the DBR mirrors. We observe significantly reduced PL background when collecting from the grating compared to when the PL is collected from the top of the cavity (see Supporting Information). By fitting a Lorentzian curve to the cavity peaks in the PL spectrum, we find line widths that correspond to a Q factor of 830 and 320 for device 1 and 2, respectively. These line widths agree with the line widths observed in transmission. Monolayer WSe₂ excitons have an in-plane dipole moment²⁶ and thus interact primarily with TE cavity modes. Hence, we expect monolayer WSe₂ excitonic PL to couple to a TE mode but not to a TM mode. Indeed, the measured cavity coupled 2D material excitonic PL from device 2 (Figure 5b) confirms our understanding as no cavity coupling is observed with the higher energy TM mode, which still lies within the excitonic spectral range. However, in Figure 5a, we observe coupling of the defect states of WSe₂ with the TM cavity mode (device 1). The defect states of WSe₂ have been a topic of significant research effort in recent years and are particularly interesting due to their single-emitter-like properties at cryogenic temperatures.^{27–30} These defects are also known to have in-plane linearly polarized emission²⁸ and hence should couple to the TE mode and not TM mode. We attribute the coupling with the TM mode to the warping of the monolayer around the SiN nanobeam (see Supporting Information). In that way, the defects still emit in the plane of the 2D materials but couple to the TM mode of the cavity. Such warping strains the monolayer, and strain-induced defect formation has been observed by several research groups in the past.^{29,31} Hence, there is a high likelihood that the defects are created due to warping of the monolayer and thus couple to the TM mode of the cavity.

DISCUSSION

We demonstrated the operation of an encapsulated SiN nanobeam despite the low index contrast between the SiN, and the material it is encapsulated within. Encapsulation provides the desired mechanical stability, which is crucial to build a hybrid optoelectronic platform with emerging materials integrated on passive integrated photonic circuits. Such stability is absent in conventional floating membranes of SiN nanobeam resonators. Our analysis shows that such encapsulation results in a 5-fold increase of the mode-volume, but the Q factor of the cavity can still reach up to $\sim 10^5$. To demonstrate the efficacy of

the developed resonators for 2D material integration, we integrated our resonators with monolayer WSe₂ and observed cavity coupled PL from both the 2D exciton and the defects embedded in the 2D materials. Going beyond layered 2D materials, we envision the encapsulated SiN nanobeams can be used to enhance the light–matter interaction with other emerging nanomaterials, such as solution processed emitters and chromophores,³² as well as perovskites.³³ We note that the encapsulation naturally provides a way to preserve materials that are sensitive to environmental conditions. By virtue of their simultaneous small mode-volumes and mechanical robustness, encapsulated SiN nanobeam resonators will provide a useful tool to develop hybrid large-scale photonic integrated circuits, with applications in optical information science and sensing.

■ ASSOCIATED CONTENT

● Supporting Information

The Supporting Information is available free of charge on the ACS Publications website at DOI: [10.1021/acsphtonic.8b00036](https://doi.org/10.1021/acsphtonic.8b00036).

Broken floating membranes; high *Q* factor NIR cavity resonances; encapsulated SiN nanobeam resonators at the telecommunications band; effect of PC and PMMA as encapsulation layer; comparison between the PL from the top and grating; design of the grating; wrapping of the 2D material; transmission spectrum of cavities with different parameters; surface roughness of the silicon nitride; emission of WSe₂ from a bare substrate (PDF)

■ AUTHOR INFORMATION

Corresponding Author

*E-mail: arka@uw.edu.

ORCID

Taylor K. Fryett: [0000-0001-7025-7352](https://orcid.org/0000-0001-7025-7352)

Author Contributions

T.K.F. conceived the idea. Y.C. performed the simulation. T.K.F. fabricated the SiN resonator. T.K.F. and Y.C. fabricated the 2D material-cavity device. J.W. and Z.M.P. helped with finding the 2D materials and transferring them. T.K.F. and Y.C. performed the optical characterization. T.K.F. wrote the paper with input from everyone. X.X. and A.M. supervised the whole project.

Notes

The authors declare no competing financial interest.

■ ACKNOWLEDGMENTS

We thank Mr. Richard Bojko and Mr. Alan Zhan for helpful discussion about SiN fabrication. This work is supported by the National Science Foundation under grant NSF-EFRI-1433496, NSF MRSEC 1719797, the Air Force Office of Scientific Research-Young Investigator Program under grant FA9550-15-1-0150 and grant FA9550-18-1-0104. All the fabrication processes were performed at the Washington Nanofabrication Facility (WNF), a National Nanotechnology Infrastructure Network (NNIN) site at the University of Washington, which is supported in part by the National Science Foundation (awards 0335765 and 1337840), the Washington Research Foundation, the M. J. Murdock Charitable Trust, GCE Market, Class One Technologies, and Google.

■ REFERENCES

- (1) Abel, S.; Stöferle, T.; Marchiori, C.; Rossel, C.; Rossell, M. D.; Erni, R.; Caimi, D.; Sousa, M.; Chelnokov, A.; Offrein, B. J.; Fompeyrine, J. *Nat. Commun.* **2013**, *4*, 1671.
- (2) Chen, R.; Tran, T.-T. D.; Ng, K. W.; Ko, W. S.; Chuang, L. C.; Sedgwick, F. G.; Chang-Hasnain, C. *Nat. Photonics* **2011**, *5* (3), 170–175.
- (3) Xia, F.; Wang, H.; Xiao, D.; Dubey, M.; Ramasubramanian, A. *Nat. Photonics* **2014**, *8* (12), 899–907.
- (4) Youngblood, N.; Li, M. Integration of 2D materials on a silicon photonics platform for optoelectronics applications. *Nanophotonics* **2016**, *6*, 0155.
- (5) Phare, C. T.; Daniel Lee, Y.-H.; Cardenas, J.; Lipson, M. *Nat. Photonics* **2015**, *9* (8), 511–514.
- (6) Wei, G.; Stanev, T.; Stern, N.; Czaplowski, D.; Jung, W. In *Interfacing Monolayer MoS₂ with Silicon-Nitride Integrated Photonics*, Advanced Photonics 2015, Boston, Massachusetts, 2015/06/27, 2015; Optical Society of America: Boston, MA, p IM4A.3.
- (7) Reed, J. C.; Malek, S. C.; Yi, F.; Naylor, C. H.; Johnson, A. T. C.; Cubukcu, E. *Appl. Phys. Lett.* **2016**, *109* (19), 193109.
- (8) Ye, Y.; Wong, Z. J.; Lu, X.; Zhu, H.; Chen, X.; Wang, Y.; Zhang, X. *Nat. Photonics* **2015**, *9*, 733–737.
- (9) Wu, S.; Buckley, S.; Jones, A. M.; Ross, J. S.; Ghimire, N. J.; Yan, J.; Mandrus, D. G.; Yao, W.; Hatami, F.; Vučković, J.; Majumdar, A.; Xu, X. *2D Mater.* **2014**, *1* (1), 011001.
- (10) Wu, S.; Buckley, S.; Schaibley, J. R.; Feng, L.; Yan, J.; Mandrus, D. G.; Hatami, F.; Yao, W.; Vučković, J.; Majumdar, A.; Xu, X. *Nature* **2015**, *520*, 69–72.
- (11) Gan, X.; Gao, Y.; Fai Mak, K.; Yao, X.; Shiu, R.-J.; van der Zande, A.; Trusheim, M. E.; Hatami, F.; Heinz, T. F.; Hone, J.; Englund, D. *Appl. Phys. Lett.* **2013**, *103* (18), 181119.
- (12) Liu, C.-H.; Clark, G.; Fryett, T.; Wu, S.; Zheng, J.; Hatami, F.; Xu, X.; Majumdar, A. *Nano Lett.* **2017**, *17*, 200.
- (13) Fryett, T. K.; Seyler, K. L.; Zheng, J.; Liu, C.-H.; Xu, X.; Majumdar, A. arXiv:1607.03548 2016.
- (14) Gan, X.; Zhao, C.; Hu, S.; Wang, T.; Song, Y.; Li, J.; Zhao, Q.; Jie, W.; Zhao, J. arXiv:1706.07923 2017.
- (15) Khan, M.; Babinec, T.; McCutcheon, M. W.; Deotare, P.; Loncar, M. *Opt. Lett.* **2011**, *36* (3), 421–423.
- (16) Khan, M.; Babinec, T.; McCutcheon, M. W.; Deotare, P.; Loncar, M. *Opt. Lett.* **2011**, *36* (3), 421–423.
- (17) Hammer, S.; Mangold, H.-M.; Nguyen, A. E.; Martinez-Ta, D.; Alvililar, S. N.; Bartels, L.; Krenner, H. J. arXiv:1706.10134 2017.
- (18) Wang, X.; Jones, A. M.; Seyler, K. L.; Tran, V.; Jia, Y.; Zhao, H.; Wang, H.; Yang, L.; Xu, X.; Xia, F. *Nat. Nanotechnol.* **2015**, *10* (6), 517–521.
- (19) Li, Y.; Zhang, J.; Huang, D.; Sun, H.; Fan, F.; Feng, J.; Wang, Z.; Ning, C. Z. *Nat. Nanotechnol.* **2017**, *12*, 987.
- (20) Johnson, S. G.; Joannopoulos, J. D. *Opt. Express* **2001**, *8* (3), 173–190.
- (21) Panettieri, D.; Faolain, L. O.; Grande, M. Control of *Q*-factor in nanobeam cavities on substrate. *2016 18th International Conference on Transparent Optical Networks (ICTON)*, 10–14 July 2016, 2016; pp 1–4.
- (22) McCutcheon, M. W.; Loncar, M. *Opt. Express* **2008**, *16* (23), 19136–19145.
- (23) Beadie, G.; Brindza, M.; Flynn, R. A.; Rosenberg, A.; Shirk, J. S. *Appl. Opt.* **2015**, *54* (31), F139–F143.
- (24) Zomer, P. J.; Guimarães, M. H. D.; Brant, J. C.; Tombros, N.; van Wees, B. J. *Appl. Phys. Lett.* **2014**, *105* (1), 013101.
- (25) Li, Y.; Chernikov, A.; Zhang, X.; Rigosi, A.; Hill, H. M.; van der Zande, A. M.; Chenet, D. A.; Shih, E.-M.; Hone, J.; Heinz, T. F. *Phys. Rev. B: Condens. Matter Mater. Phys.* **2014**, *90* (20), 205422.
- (26) Schuller, J. A.; Karaveli, S.; Schiros, T.; He, K.; Yang, S.; Kyymissis, I.; Shan, J.; Zia, R. *Nat. Nanotechnol.* **2013**, *8* (4), 271–276.
- (27) Srivastava, A.; Sidler, M.; Allain, A. V.; Lembke, D. S.; Kis, A.; Imamoglu, A. *Nat. Nanotechnol.* **2015**, *10* (6), 491–496.

(28) He, Y.-M.; ClarkGenevieve; SchaibleyJohn, R.; He, Y.; ChenMing, C.; WeiYu, J.; Ding, X.; Zhang, Q.; Yao, W.; Xu, X.; Lu, C.-Y.; Pan, J.-W. *Nat. Nanotechnol.* **2015**, *10* (6), 497–502.

(29) Palacios-Berraquero, C.; Kara, D. M.; Montblanch, A. R. P.; Barbone, M.; Latawiec, P.; Yoon, D.; Ott, A. K.; Loncar, M.; Ferrari, A. C.; Atatüre, M. *2017*, *8*, 15093.

(30) Palacios-Berraquero, C.; Barbone, M.; Kara, D. M.; Chen, X.; Goykhman, I.; Yoon, D.; Ott, A. K.; Beitner, J.; Watanabe, K.; Taniguchi, T.; Ferrari, A. C.; Atatüre, M. *2016*, *7*, 12978.

(31) Branny, A.; Kumar, S.; Proux, R.; Gerardot, B. D. *Nat. Commun.* **2017**, *8*, 15053.

(32) Dai, X.; Zhang, Z.; Jin, Y.; Niu, Y.; Cao, H.; Liang, X.; Chen, L.; Wang, J.; Peng, X. *Nature* **2014**, *515* (7525), 96–99.

(33) Sutherland, B. R.; Sargent, E. H. *Nat. Photonics* **2016**, *10* (5), 295–302.